



# CHORUS

This is the accepted manuscript made available via CHORUS. The article has been published as:

## Efficient sampling avoids the exponential wall in classical simulations of fidelity

Cesare Mollica, Tomáš Zimmermann, and Jiří Vaníček

Phys. Rev. E **84**, 066205 — Published 14 December 2011

DOI: [10.1103/PhysRevE.84.066205](https://doi.org/10.1103/PhysRevE.84.066205)

# Efficient sampling avoids the exponential wall in classical simulations of fidelity

Cesare Mollica, Tomáš Zimmermann, and Jiří Vaníček\*

*Laboratory of Theoretical Physical Chemistry,*

*Institut des Sciences et Ingénierie Chimiques,*

*Ecole Polytechnique Fédérale de Lausanne, Lausanne, Switzerland*

## Abstract

We analyze the efficiency of available algorithms for the simulation of classical fidelity and show that their computational costs increase exponentially with the number of degrees of freedom. Then we present an algorithm for which the number of trajectories needed for convergence is independent of the system's dimensionality and show that, within a continuous family of algorithms, this algorithm is the only one with this property. Simultaneously we propose a general analytical approach to estimate efficiency of trajectory-based methods and suggest how to use it to accelerate calculations of other classical correlation functions. Converged numerical results are provided for systems with phase space volume  $2^{1700}$  times larger than the volume of the initial state.

PACS numbers: 05.45.-a, 05.45.Jn, 05.45.Mt, 05.45.Pq

---

\* [jiri.vanicek@epfl.ch](mailto:jiri.vanicek@epfl.ch)

*Introduction.* While the solution of the time-dependent Schrödinger equation scales exponentially with dimensionality and is feasible for only a few continuous degrees of freedom (DOF), classical molecular dynamics simulations are, in principle, feasible for millions of atoms. It may therefore be surprising that studies of classical fidelity have provided numerical results for only one or a few DOF [1–4]. A notable exception is Ref. [5], which, for the largest systems, relies on initial densities given by characteristic functions. Below we explain this situation by showing that for initial Gaussian densities, not only quantum but also all previously used classical algorithms for fidelity scale exponentially with the number  $D$  of DOF. Hence even when quantum effects are negligible and classical picture is appropriate, the “simple” classical simulations may be unfeasible. Since numerical simulations are important for testing analytical theories of classical fidelity in large systems, we design an efficient classical fidelity algorithm that avoids the exponential scaling with  $D$ .

*Classical and quantum fidelity.* Classical fidelity is important both as a theoretical measure of stability of classical dynamics [1–5] and as a practical tool to measure the accuracy of classical molecular dynamics with an approximate many-body Hamiltonian (e.g., a “force field”) [6]. While important in its own right, classical fidelity can be viewed as the classical limit of quantum fidelity [7], introduced by Peres [8] to measure the stability of quantum dynamics. Quantum fidelity is the squared overlap  $F_{\text{QM}}(t)$  at time  $t$  of two quantum states, identical at  $t = 0$ , but evolved with two different Hamiltonians,  $H_0$  and  $H_\epsilon = H_0 + \epsilon V$ :

$$F_{\text{QM}}(t) := |f_{\text{QM}}(t)|^2, \tag{1}$$

$$f_{\text{QM}}(t) := \langle \psi | U_\epsilon^{-t} U_0^t | \psi \rangle, \tag{2}$$

where  $f_{\text{QM}}(t)$  is the quantum fidelity amplitude and  $U_\epsilon^t := \exp(-iH_\epsilon t/\hbar)$  the quantum evolution operator. Rewriting Eq. (2) as  $f_{\text{QM}}(t) = \langle \psi | U^t | \psi \rangle$  with the echo operator  $U^t := U_\epsilon^{-t} U_0^t$ , it can be interpreted as the Loschmidt echo, i.e., an overlap of an initial state with a state evolved for time  $t$  with  $H_0$  and subsequently for time  $-t$  with  $H_\epsilon$ . (In general, we write time  $t$  as a superscript. Subscript  $\epsilon$  denotes that  $H_\epsilon$  was used for dynamics. If an evolution operator, phase space coordinate, or density lacks a subscript, Loschmidt echo dynamics is implied.) Quantum fidelity has many applications, e.g., in NMR spin echo experiments [9], neutron scattering [10], ultrafast electronic spectroscopy [11], quantum computation and decoherence [12], and as a measure of nonadiabaticity [13] or accuracy of molecular quantum dynamics on an approximate potential energy surface [6].

For simplicity, we first assume that the initial states are pure and defer the generalization to mixed states and other phase space densities to a later section. One can rewrite quantum fidelity (1) as  $F_{\text{QM}}(t) = \text{Tr}(\hat{\rho}_\epsilon^t \hat{\rho}_0^t)$ , where  $\hat{\rho}_\epsilon^t := U_\epsilon^t \hat{\rho} U_\epsilon^{-t}$  is the density operator at time  $t$ . In the phase-space formulation of quantum mechanics, quantum fidelity becomes  $F_{\text{QM}}(t) = h^{-D} \int dx \rho_{\epsilon, \text{W}}^t(x) \rho_{0, \text{W}}^t(x)$ , where  $x := (q, p)$  is a point in phase space and  $A_{\text{W}}(x) := \int d\xi \langle q - \xi/2 | A | q + \xi/2 \rangle e^{ip\xi/\hbar}$  is the Wigner transform of  $A$ . This form of quantum fidelity suggests directly its classical limit, which is precisely the classical fidelity, defined as [1, 2]

$$F_{\text{CL}}(t) := F_{\text{fid}}(t) = h^{-D} \int dx \rho_\epsilon^t(x) \rho_0^t(x) \quad (3)$$

$$= F_{\text{echo}}(t) = h^{-D} \int dx \rho^t(x) \rho^0(x) \quad (4)$$

where the first and second line express classical fidelity in the fidelity and Loschmidt echo pictures, respectively,  $\rho_\epsilon^t$  is the classical phase-space density evolved with  $H_\epsilon$ , and  $\rho^t$  is this density evolved under the echo dynamics. While expressions (3)-(4) are completely classical, the phase-space volume is measured in units of  $h^D$  to make the quantum-classical correspondence explicit. We omit subscript ‘‘CL’’ for classical quantities  $F$  and  $\rho$  since classical fidelity is the main subject of this paper.

*Algorithms.* The exponential scaling of quantum dynamics with  $D$  is well known. As for classical fidelity, Eqs. (3)-(4) may be evaluated, e.g., with trajectory, grid, or mesh-based methods. Clearly, the grid-based methods would suffer from an exponential scaling as quantum dynamics on a grid. We focus on the most general and straightforward trajectory-based methods, obtained from Eqs. (3)-(4) using the Liouville theorem, yielding equivalent expressions

$$F_{\text{fid}}(t) = h^{-D} \int dx^0 \rho(x_\epsilon^{-t}) \rho(x_0^{-t}) \quad \text{and} \quad (5)$$

$$F_{\text{echo}}(t) = h^{-D} \int dx^0 \rho(x^{-t}) \rho(x^0). \quad (6)$$

Above,  $x_\epsilon^t := \Phi_\epsilon^t(x^0)$ , where  $\Phi_\epsilon^t$  is the Hamiltonian flow of  $H_\epsilon$ , and  $x^t := \Phi^t(x^0)$ , where  $\Phi^t := \Phi_\epsilon^{-t} \circ \Phi_0^t$  is the Loschmidt echo flow. Since it is the phase space points rather than the densities that evolve in expressions (5)-(6), we can take  $\rho = \rho_{\text{W}}$ , i.e., the Wigner transform of the initial quantum state. We further rewrite Eqs. (5)-(6) in a form suitable for Monte Carlo evaluation, i.e., as an average

$$\langle A(x^0, t) \rangle_{W(x^0)} := \frac{\int dx^0 A(x^0, t) W(x^0)}{\int dx^0 W(x^0)}$$

where  $W$  is the sampling weight for initial conditions  $x^0$ . The weight can be any positive definite function but it is advantageous to consider the weight to be related to the density  $\rho$ . While previously used algorithms sampled from  $\rho$  [2, 4, 5], we consider more general weights  $W = W_M(x^0) := \rho(x^0)^M$  and  $W = W_M(x_0^{-t}) = \rho(\Phi_0^{-t}(x^0))^M$  for the echo and fidelity dynamics, respectively. These weights yield  $M$ -dependent algorithms

$$F_{\text{fid-}M}(t) = I_M \langle \rho(x_\epsilon^{-t}) \rho(x_0^{-t})^{1-M} \rangle_{\rho(x_0^{-t})^M}, \quad (7)$$

$$F_{\text{echo-}M}(t) = I_M \langle \rho(x^{-t}) \rho(x^0)^{1-M} \rangle_{\rho(x^0)^M}, \quad (8)$$

where  $I_M := h^{-D} \int \rho(x^0)^M dx^0$  is a normalization factor. In both families of algorithms (7)-(8), sampling can be done by Metropolis Monte Carlo for general dynamics and any positive definite weight  $\rho^M$ . For  $M > 0$ , the echo algorithms (8) are, however, much more practical since the initial state is often known explicitly (and generally is much smoother than the final state), making sampling easier. Furthermore, for simple initial states such as Gaussian wavepackets (GWPs), the Metropolis sampling in the echo algorithms can be replaced by analytical sampling. Therefore, for  $M > 0$  the fidelity algorithms are more of a theoretical possibility than a practical tool. For  $M = 0$ , the sampling is uniform and makes sense only for a compact phase space of finite volume  $\Omega = \Omega_1^D = (n_1 h)^D$ , where  $\Omega_1$  and  $n_1$  are respectively the phase space volume and Hilbert-space dimension for a single DOF. For  $M > 0$ , importance sampling based on the weight  $W_M$  is used and an infinite phase space is allowed. For general  $M$ , the sampling is only defined for classical states (such as GWPs), for which  $\rho \geq 0$ . However, for  $M = 0$  and for the important special case of  $M = 2$ , the sampling is defined for any state, i.e., even for negative values of  $\rho$ .

In order to compute classical fidelity directly from algorithms (7) or (8), the normalization factor  $I_M$  must be known analytically. For general pure states,  $I_M$  is known analytically only for  $M = 0, 1$ , or  $2$ . For  $M = 0$ ,  $I_0 = n_1^D$  because of the requirement of finite phase space. For both  $M = 1$  and  $M = 2$ ,  $I_M = 1$  since  $\text{Tr } \hat{\rho} = \text{Tr } \hat{\rho}^2 = 1$ . For  $M \notin \{0, 1, 2\}$ , algorithms (7) and (8) can only be used for special initial states. E.g., for initial GWPs  $\rho(x) = g(x; X, a) := 2^D \exp[-(q - Q)^2/a^2 - (p - P)^2 a^2/\hbar^2]$ , where  $X$  is the center and  $a$  the width of the GWP, we have  $I_M = (2^{M-1}/M)^D$  for general  $M > 0$ . However, the unknown normalization factor can be removed from Eqs. (7) and (8) by dividing them by the value of  $I_2$  [note that  $I_2(0) = F(0)$ ]

obtained with the same algorithm and trajectories. Resulting “normalized” (N) algorithms,

$$F_{\text{fid-N-M}}(t) = \frac{\langle \rho(x_\epsilon^{-t}) \rho(x_0^{-t})^{1-M} \rangle_{\rho(x_0^{-t})^M}}{\langle \rho(x_0^{-t})^{2-M} \rangle_{\rho(x_0^{-t})^M}}, \quad (9)$$

$$F_{\text{echo-N-M}}(t) = \frac{\langle \rho(x^{-t}) \rho(x^0)^{1-M} \rangle_{\rho(x^0)^M}}{\langle \rho(x^0)^{2-M} \rangle_{\rho(x^0)^M}}, \quad (10)$$

are practical for general initial states and for any  $M$ . As far as we know, from the four families of algorithms (7), (8), (9), and (10) only echo-1 (8) has been used previously [2, 4, 5]. Note, however, that for initial densities given by characteristic functions (which may not necessarily correspond to quantum states), echo-1 = echo- $M$  = echo-N- $M$  for all  $M > 0$ .

*Efficiency.* The cost of a typical method propagating  $N$  trajectories for time  $t$  is  $O(c_f t N)$ , where  $c_f$  is the cost of a single force evaluation. However, among the above mentioned algorithms, this is only true for the fidelity algorithms with  $M = 0$ . Remarkably, in all other cases, the cost is  $O(c_f t^2 N)$ . For a single time  $t$ , the cost is linear in time, but if one wants to know classical fidelity for all times up to  $t$ , the cost is quadratic with  $t$ . For the echo algorithms, it is because one must make full backward propagation for each time between 0 and  $t$ . For the fidelity algorithms, it is because the weight function  $\rho(x^{-t})^M$  changes with time and the sampling has to be redone from scratch for each time between 0 and  $t$ . In other words, different trajectories are used for each time between 0 and  $t$ .

The above estimates are correct but not the full story. There are hidden costs since the number of trajectories  $N$  required for convergence can depend on  $D$ ,  $t$ , dynamics, initial state, and method. One usually empirically increases  $N$  until convergence but this is often impracticable. Instead, we estimate  $N$  analytically. An essential point is that  $N$  is fully determined by the desired discretization error  $\sigma_{\text{discr}}$ . The expected systematic component of  $\sigma_{\text{discr}}$  is zero or  $O(N^{-1})$  for all cases studied and is negligible to the expected statistical component  $\sigma = O(N^{-1/2})$  which therefore determines convergence. This statistical error is computed as  $\sigma^2(t, N) = \overline{F(t, N)^2} - \overline{F(t, N)}^2$ , the overline denoting an average over infinitely many independent simulations with  $N$  trajectories. Hence we can formulate the problem of efficiency precisely: “What  $N$  is required to converge fidelity  $F$  to within a statistical error  $\sigma$ ?” We let  $N$  be a function of  $F$  because in many applications, one is interested in  $F$  above a certain threshold value  $F_{\text{min}}$ . This threshold can vary with application: It may be close to unity (in quantum computing, where high fidelity is required independently of  $D$ ) or to zero (yet finite, in calculations of spectra as Fourier transforms of fidelity which must be known with certain precision independent of  $D$ ). Quite generally, the threshold will

be *independent* of  $D$ . Moreover, as will turn out below, expressing  $N$  as a function of  $F$  permits obtaining general expressions valid for any dynamics.

The discretized form of Eq. (7) is  $F_{\text{fid-}M}(t, N) = I_M N^{-1} \sum_{j=1}^N \rho(x_{\epsilon, j}^{-t}) \rho(x_{0, j}^{-t})^{1-M}$ , from which

$$\begin{aligned} \overline{F_{\text{fid-}M}(t, N)^2} &= I_M^2 N^{-1} \langle \rho(x_{\epsilon}^{-t})^2 \rho(x_0^{-t})^{2-2M} \rangle_{\rho(x_0^{-t})^M} \\ &\quad + (1 - N^{-1}) F^2. \end{aligned}$$

Similarly, from Eq. (8)  $F_{\text{echo-}M}(t, N) = I_M N^{-1} \sum_{j=1}^N \rho(x_j^{-t}) \rho(x_j^0)^{1-M}$ , hence

$$\begin{aligned} \overline{F_{\text{echo-}M}(t, N)^2} &= I_M^2 N^{-1} \langle \rho(x^{-t})^2 \rho(x^0)^{2-2M} \rangle_{\rho(x^0)^M} \\ &\quad + (1 - N^{-1}) F^2. \end{aligned}$$

Realizing that  $\overline{F_{\text{fid-}M}(t, N)} = \overline{F_{\text{echo-}M}(t, N)} = F(t)$  in both cases, we obtain the same error

$$\sigma_{\text{fid-}M}^2 = \sigma_{\text{echo-}M}^2 = N^{-1} (I_M J_M - F^2), \quad (11)$$

$$J_M := h^{-D} \int dx^0 \rho(x^{-t})^2 \rho(x^0)^{2-M}. \quad (12)$$

In the special case of  $M = 2$ , we find our *first major result*,

$$\sigma_{\text{fid-}2}^2 = \sigma_{\text{echo-}2}^2 = N^{-1} (1 - F^2). \quad (13)$$

This expression shows that for general pure states and for general dynamics, statistical errors of  $F_{\text{fid-}2}$  and  $F_{\text{echo-}2}$  depend only on  $N$  and  $F$ . In other words, the number of trajectories needed for convergence is *independent* of  $t$ ,  $D$ , or dynamics of the system. This important result is due to the fact that for the sampling weight  $W = \rho^2$ , each numerical trajectory contributes evenly to the weighted average (at time  $t = 0$ ).

As for algorithms (7)-(8) with  $M \neq 2$ , one might hope to improve convergence by employing the normalized versions (9)-(10). The error analysis is simplified using the formula for statistical error of a ratio of two random variables,

$$\left( \frac{\sigma_{A/B}}{A/B} \right)^2 = \left( \frac{\sigma_A}{A} \right)^2 + \left( \frac{\sigma_B}{B} \right)^2 - 2 \frac{\overline{AB} - \bar{A}\bar{B}}{AB}. \quad (14)$$

In our case,  $F_{N-M}(t, N) = A/B$ , where  $A = F_M(t, N)$ ,  $B = F_M(0, N)$ ,  $\bar{A} = F(t)$ ,  $\bar{B} = F(0) = 1$ , and  $\sigma_A$  and  $\sigma_B$  are given by Eq. (11). The only unknown in Eq. (14) is  $\overline{AB}$ . For the normalized

echo algorithms (10), we have

$$\begin{aligned}
\overline{AB} &= \overline{F_{\text{echo-}M}(t, N)F_{\text{echo-}M}(0, N)} \\
&= I_M^2 N^{-1} \langle \rho(x^{-t})\rho(x^0)^{3-2M} \rangle_{\rho(x^0)^M} \\
&\quad + (1 - N^{-1})F(t)F(0) \\
&= N^{-1}I_M K_M + (1 - N^{-1})F,
\end{aligned}$$

where  $K_M := h^{-D} \int dx^0 \rho(x^{-t})\rho(x^0)^{3-M}$ . The same derivation goes through for the fidelity algorithms. In both cases, the error is

$$\sigma_{N-M}^2 = N^{-1}I_M (J_M - 2K_M F + I_{4-M}F^2). \quad (15)$$

*Exponential growth of the error for  $M \neq 2$ .* Now we will show that the special case  $M = 2$  is unique and that all the other above-mentioned algorithms (which include all the algorithms available in the literature) may have an error growing exponentially with  $D$ . Since we are searching for counterexamples, special cases are sufficient. For us these will be initial GWP states and ‘‘pure displacement’’ (PD) or ‘‘pure squeezing’’ (PS) dynamics [3].

In the PD case, the center of the GWP moves while both its shape and size remain constant. Such fidelity dynamics can be realized exactly by two displaced simple harmonic oscillator (SHO) potentials with equal force constants. For PD, the width  $a^t = a^0 = a$  and  $X^t = X^0 + \Delta X^t$ . classical fidelity is  $F(t) = h^{-D} \int dx g(x; X^t, a)g(x; X^0, a) = \exp \left\{ -\frac{1}{2} \left[ \left( \frac{\Delta Q^t}{a} \right)^2 + \left( \frac{\Delta P^t a}{\hbar} \right)^2 \right] \right\}$  and the factor (12) can be expressed in terms of  $F$  as  $J_M = \left( \frac{2^{3-M}}{4-M} \right)^D F^{\gamma_M}$  with  $\gamma_M = 4 - 8/(4 - M)$ , reducing statistical error (11) to

$$\sigma_{M, \text{PD}}^2 = N^{-1} (\beta_M^D F^{\gamma_M} - F^2), \quad (16)$$

$$\beta_0 = 2n_1 \text{ and } \beta_{0 < M < 4} = \frac{4}{(4 - M)M}. \quad (17)$$

The error diverges for  $M \geq 4$ . Note that  $\beta_M \geq 1$  and the minimum  $\beta_2 = 1$ , achieved for  $M = 2$ , agrees with the general result (13). Except for  $M = 2$ ,  $\beta_M > 1$ , showing that even in the simple case of PD, errors of all algorithms from families (7) and (8) grow *exponentially* with  $D$ , which is the *second major result* of this paper. Normalized methods (9) and (10) lower the prefactor but do not change the exponential scaling with  $D$ : Since  $K_M = [2^{3-M}/(4 - M)]^D F^{\delta_M}$ , where  $\delta_M = 2 - 2/(4 - M)$ , the statistical error is

$$\sigma_{N-M, \text{PD}}^2 = N^{-1} \beta_M^D (F^{\gamma_M} - 2F^{1+\delta_M} + F^2).$$

In the PS case, the center of the GWP remains fixed while its width narrows in some directions and spreads in others. PS dynamics is realized by two inverted SHOs with common centers and different force constants. For  $0 < M < 4$ ,

$$\sigma_{M, \text{PS}}^2 = N^{-1} (\beta_M^D R^{-D/2} - F^2), \quad (18)$$

$$\sigma_{N-M, \text{PS}}^2 = N^{-1} \beta_M^D (R^{-D/2} - 2T^{-D/2}F + F^2), \quad (19)$$

where  $R := 1 + \rho_M (F^{-2/D} - 1)$ ,  $T := 1 + \tau_M (F^{-2/D} - 1)$ ,  $\rho_M := 8(2 - M)/(4 - M)^2$ , and  $\tau_M := 4(3 - M)/(4 - M)^2$ . For  $D \rightarrow \infty$ , these errors grow as

$$\sigma_{M, \text{PS}}^2 \sim N^{-1} (\beta_M^D F^{\rho_M} - F^2), \quad (20)$$

$$\sigma_{N-M, \text{PS}}^2 \sim N^{-1} \beta_M^D (F^{\rho_M} - 2F^{1+\tau_M} + F^2), \quad (21)$$

increasing *exponentially* with  $D$  for all  $M$  except  $M = 2$ . The errors diverge always for  $M \geq 4$  but, depending on  $F$  and  $D$ , may diverge for any  $M > 2$ .

To summarize, in all cases studied, for  $D \gg 1$  the number of trajectories required for a specified convergence is

$$N = \sigma^{-2} \alpha(F) \beta^D \quad (22)$$

where  $\alpha$  and  $\beta$  depend on the method and dynamics and are listed in Table I for the most important special cases. For both fidelity and echo algorithms with  $M = 2$ , for any dynamics and any initial state, the coefficient  $\beta = 1$ , implying independence of  $D$ . Note also that algorithms with  $M = 2$  are automatically normalized. For all other algorithms (both echo and fidelity, both unnormalized and normalized, and for any  $M \neq 2$ ) and for both PD and PS dynamics,  $\beta > 1$ , implying an exponential growth with  $D$ . This growth is dramatic for  $M = 0$  ( $\beta = 2n_1 \gg 1$ ): since  $n_1^D$  is the Hilbert space dimension, the cost of  $M = 0$  algorithms approaches that of quantum fidelity. This is unfortunate since  $F_{\text{fid},0}$  is the only algorithm that scales linearly with time. On the other hand, for the most intuitive and most common  $M = 1$  algorithms,  $\beta = 4/3$ , and the growth is much slower, although still exponential.

*Mixed states and general phase space densities.* Definitions of quantum or classical fidelity can be generalized to mixed states in different ways [7, 14]. Keeping definitions (3)-(4) also for classical fidelity of mixed states, expression (11) remains unchanged. For  $M = 2$ ,  $\sigma_2^2 = N^{-1} (P^2 - F^2)$ , where  $P = h^{-D} \int dx \rho(x)^2$  is the purity, and the error is again independent of  $D$ . Since for mixed states  $F < 1$  even at  $t = 0$ , classical fidelity is usually generalized as

$$\tilde{F}(t) := \frac{\int dx \rho_\epsilon^t(x) \rho_0^t(x)}{\int dx \rho_0^t(x)^2} = \frac{\int dx \rho^t(x) \rho^0(x)}{\int dx \rho^0(x)^2}, \quad (23)$$

Method	Dynamics type	$\alpha(F)$	$\beta$
fid-0	displacement	$F^2$	$2n_1$
fid-0	squeezing	$F$	$2n_1$
echo-1	displacement	$F^{4/3}$	$4/3$
echo-1	squeezing, $D \rightarrow \infty$	$F^{8/9}$	$4/3$
echo-N-1	displacement	$F^2 + F^{4/3} - 2F^{7/3}$	$4/3$
echo-N-1	squeezing, $D \rightarrow \infty$	$F^2 + F^{8/9} - 2F^{17/9}$	$4/3$
echo-2	general, general state	$1 - F^2$	1

TABLE I. The number of trajectories needed for convergence is for  $D \gg 1$  given by  $N = \sigma^{-2}\alpha(F)\beta^D$ . The table lists  $\alpha(F)$  and  $\beta$  for important special cases. Note that fid-0, echo-1, and echo-N-1 results are for initial GWPs and scale exponentially with  $D$  while the echo-2 result, valid for any initial density, is independent of  $D$ .

giving  $\tilde{F} = 1$  at  $t = 0$ . This definition works for any normalized phase space density (even with  $P > 1$ ). Evaluating Eq. (23) with fid-N- $M$  or echo-N- $M$  algorithms gives

$$\tilde{\sigma}_{N-M}^2 = N^{-1} \frac{I_M}{P^2} \left( J_M - 2K_M \tilde{F} + I_{4-M} \tilde{F}^2 \right). \quad (24)$$

For  $M = 2$ , the error is independent of  $D$  for any normalized phase space density since  $\tilde{\sigma}_{N-2}^2 = N^{-1} \left( 1 - \tilde{F}^2 \right)$ , which is the *third major result* of this paper.

*Numerical results and conclusion.* To illustrate the analytical results obtained above, numerical tests were performed in multidimensional systems of uncoupled displaced SHOs (for PD dynamics), inverted SHOs (for PS dynamics), and perturbed kicked rotators (for generic nonlinear integrable and chaotic dynamics). The last model is defined,  $\text{mod}(2\pi)$ , by the map  $q_{j+1} = q_j + p_j$ ,  $p_{j+1} = p_j - \nabla W(q_{j+1}) - \epsilon \nabla V(q_{j+1})$ , where  $W(q) = -k \cos q$  is the potential and  $V(q) = -\cos(2q)$  the perturbation of the system;  $k$  and  $\epsilon$  determine the type of dynamics and perturbation strength, respectively. Uncoupled systems were used in order to make quantum fidelity calculations feasible (as a product of  $D$  1-dimensional calculations); however, the classical fidelity calculations were performed as for a truly  $D$ -dimensional system. The initial state was always a multidimensional GWP, with  $X = (0.1, 0.9) \cdot 2\pi$ ,  $a = \sqrt{\hbar}$  (in Fig. 1) or  $X = (1/2, 0)$ ,  $a = 1$  (in Fig. 2) in all dimensions. Expected statistical errors were estimated by averaging actual statistical errors over 100 different sets of  $N$  trajectories. No fitting was used in any figure, yet all numer-

ical results agree with analytical estimates. The figures show results also for algorithm echo-1',  $F_{\text{echo-1}'}(t) = 1 + \langle \rho(x^{-t}) - \rho(x^0) \rangle_{\rho(x^0)}$ , which is a variant of echo-1 accurate for high fidelity. Both echo-1 and echo-1' reduce to echo-N-1 if normalized.

Figure 1 displays fidelity in a 100-dimensional system of kicked rotators. It shows that echo-2 converges with several orders of magnitude fewer trajectories than the echo-1, echo-1', and echo-N-1 algorithms. Figure 2 confirms that  $\sigma_{\text{echo-2}}$  is independent of  $D$  while  $\sigma_{\text{echo-1}}$ ,  $\sigma_{\text{echo-1}'}$ , and  $\sigma_{\text{echo-N-1}}$  grow exponentially with  $D$ . The normalized echo-N-1 algorithm is the most efficient among the methods with  $M = 1$ .

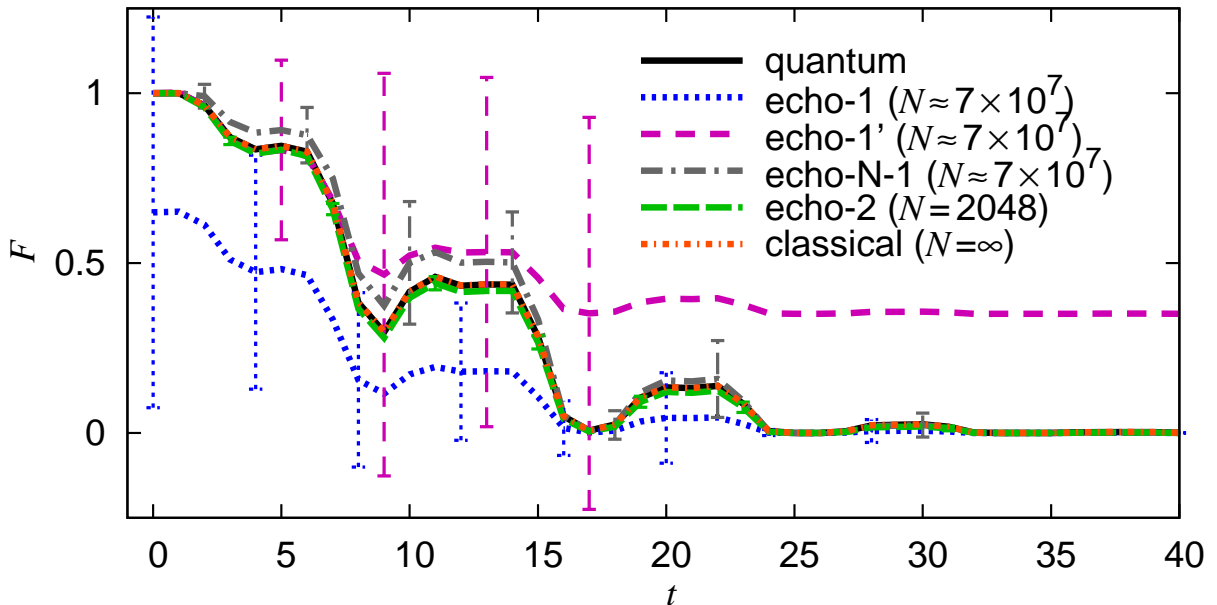


FIG. 1. (Color online) Convergence of different classical fidelity algorithms in a 100-dimensional system of perturbed ( $\epsilon = 10^{-4}$ ) quasi-integrable ( $k = 0.2$ ) kicked rotators with  $n_1 = 131072$ . Algorithm echo-2 agrees with the quantum result and converges with only  $N = 2048$  trajectories whereas the echo-1, echo-1', and echo-N-1 results are far from converged even with  $N \approx 7 \times 10^7$ . Fully converged classical ( $N = \infty$ ) result is computed as a product of 100 one-dimensional fidelities. The “hopelessly” unconverged fidelity algorithm not shown. For clarity, echo-1' error bars not shown for  $t > 20$ .

In conclusion, we have shown on the example of classical fidelity that not only quantum simulations but also classical algorithms can be unfeasible in complex systems due to the exponential scaling with dimensionality. We have proposed an efficient classical fidelity algorithm for which this exponential scaling disappears. The echo-2 algorithm makes high-dimensional studies of clas-

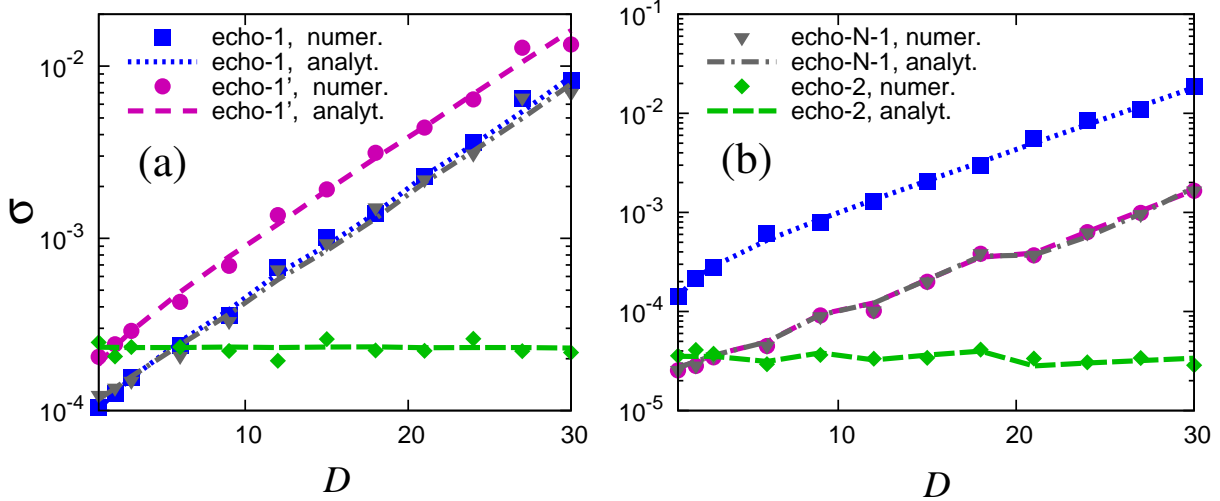


FIG. 2. (Color online) Statistical error grows exponentially with  $D$  for the echo-1, echo-1', and echo-N-1 algorithms and is independent of  $D$  for the echo-2 algorithm. Dynamics corresponds to (a) pure displacement or (b) pure squeezing. In both cases,  $N \approx 10^7$  and time was chosen separately for each  $D$  so that  $F$  is independent of  $D$ . (a)  $F \approx 0.3$ . The two SHOs had the same force constant  $k = 3$  while their displacement in each DOF decreased with increasing  $D$  from 0.8 to 0.2 (to obtain a slower decay of  $F$  per DOF for high  $D$ ). (b)  $F \approx 0.99$ . While the displacement of the unperturbed and perturbed SHOs was zero, their force constants were  $k = -3$  and  $k = -3.5$ , respectively.

sical fidelity practical for general initial densities. The algorithm thus enables, e.g., a systematic analysis of the stability of molecular dynamics to perturbations or a rigorous evaluation of the accuracy of molecular dynamics following an approximate force field. In the special case of initial densities given by characteristic functions all echo- $M$  and echo-N- $M$  algorithms (for  $M > 0$ ) collapse into a single algorithm. In particular, the “natural” algorithm sampling from  $\rho$  is equivalent to our algorithm sampling from  $\rho^2$ . This may explain why high-dimensional calculations were previously done only with characteristic functions. These results should be also useful in applications computing more general overlaps of phase space distributions. For example, the sampling weight  $W(x) \propto \rho^0(x) A^0(x) B^0(x)$  may accelerate the calculation of correlation functions of the form  $C_{AB}(t) = h^{-D} \int dx \rho^0(x) A^0(x) B^t(x)$ . Finally, the technique we used to analyze efficiency of general trajectory-based algorithms can be useful in developing approximate methods for quantum dynamics of large systems [15]. Our research was supported by Swiss NSF with grants No. 200021\_124936 and NCCR MUST, and by EPFL. We thank G. Benenti, B. Eckhardt, T. Prosen,

M. Šulc, and G. Veble for useful discussions.

---

- [1] T. Prosen and M. Žnidarič, *J. Phys. A*, **35**, 1455 (2002).
- [2] G. Benenti and G. Casati, *Phys. Rev. E*, **65**, 066205 (2002).
- [3] B. Eckhardt, *J. Phys. A*, **36**, 371 (2003); M. Combescure and A. Combescure, *J. Math. Anal. Appl.*, **326**, 908 (2007).
- [4] Z. P. Karkuszewski, C. Jarzynski, and W. H. Zurek, *Phys. Rev. Lett.*, **89**, 170405 (2002); G. Benenti, G. Casati, and G. Veble, *Phys. Rev. E*, **67**, 055202 (2003); **68**, 036212 (2003); G. Veble and T. Prosen, *Phys. Rev. Lett.*, **92**, 034101 (2004); G. Casati, T. Prosen, J. Lan, and B. Li, **94**, 114101 (2005).
- [5] G. Veble and T. Prosen, *Phys. Rev. E*, **72**, 025202 (2005).
- [6] B. Li, C. Mollica, and J. Vaníček, *J. Chem. Phys.*, **131**, 041101 (2009); T. Zimmermann, J. Ruppen, B. Li, and J. Vaníček, *Int. J. Quant. Chem.*, **110**, 2426 (2010).
- [7] T. Gorin, T. Prosen, T. H. Seligman, and M. Žnidarič, *Phys. Rep.*, **435**, 33 (2006); P. Jacquod and C. Petitjean, *Adv. Phys.*, **58**, 67 (2009).
- [8] A. Peres, *Phys. Rev. A*, **30**, 1610 (1984).
- [9] H. M. Pastawski, P. R. Levstein, G. Usaj, J. Raya, and J. Hirschinger, *Physica A*, **283**, 166 (2000).
- [10] C. Petitjean, D. V. Bevilaqua, E. J. Heller, and P. Jacquod, *Phys. Rev. Lett.*, **98**, 164101 (2007).
- [11] S. Mukamel, *J. Chem. Phys.*, **77**, 173 (1982); Z. Li, J.-Y. Fang, and C. C. Martens, **104**, 6919 (1996); S. A. Egorov, E. Rabani, and B. J. Berne, **108**, 1407 (1998); Q. Shi and E. Geva, **122**, 064506 (2005); M. Wehrle, M. Šulc, and J. Vaníček, *Chimia*, **65**, 334 (2011).
- [12] F. M. Cucchietti, D. A. R. Dalvit, J. P. Paz, and W. H. Zurek, *Phys. Rev. Lett.*, **91**, 210403 (2003); T. Gorin, T. Prosen, and T. H. Seligman, *New J. Phys.*, **6**, 20 (2004).
- [13] T. Zimmermann and J. Vaníček, *J. Chem. Phys.*, **132**, 241101 (2010); not published (2011).
- [14] J. Vaníček, *Phys. Rev. E*, **70**, 055201 (2004); **73**, 046204 (2006).
- [15] C. Mollica and J. Vaníček, *Phys. Rev. Lett.*, **107**, 214101 (2011).